Analyst

PAPER

Cite this: *Analyst*, 2017, **142**, 4089

Modeling the transformation of atmospheric CO_2 into microalgal biomass†

Mohammed Fahad Hasan and Frank Vogt *

Marine phytoplankton acts as a considerable sink of atmospheric CO_2 as it sequesters large quantities of this greenhouse gas for biomass production. To assess microalgae's counterbalancing of global warming, the quantities of CO_2 they fix need to be determined. For this task, it is mandatory to understand which environmental and physiological parameters govern this transformation from atmospheric CO_2 to microalgal biomass. However, experimental analyses are challenging as it has been found that the chemical environment has a major impact on the physiological properties of the microalgae cells (diameter typ. 5–20 μm). Moreover, the cells can only chemically interact with their immediate vicinity and thus compound sequestration needs to be studied on a microscopic spatial scale. Due to these reasons, computer simulations are a more promising approach than the experimental studies. Modeling software has been developed that describes the dissolution of atmospheric CO_2 into oceans followed by the formation of HCO_3^- which is then transported to individual microalgae cells. The second portion of this model describes the competition of different cell species for this HCO_3^-, a nutrient, as well as its uptake and utilization for cell production. Two microalgae species, *i.e. Dunaliella salina* and *Nannochloropsis oculata*, were cultured individually and in a competition situation under different atmospheric CO_2 conditions. It is shown that this novel model's predictions of biomass production are in very good agreement with the experimental flow cytometry results. After model validation, it has been applied to long-term prediction of phytoplankton generation. These investigations were motivated by the question whether or not cell production slows down as cultures grow. This is of relevance as a reduced cell production rate means that the increase in a culture's CO_2-sinking capacity slows down as well. One implication resulting from this is that an increase in anthropogenic CO_2 may not be counterbalanced by an increase in phytoplankton production. Modeling studies have found that for several different atmospheric CO_2 levels provided to single-species cultures as well as to species in competing scenarios the cell production rate does slow down over time.

Received 23rd June 2017,
Accepted 15th September 2017

DOI: 10.1039/c7an01054k

rsc.li/analyst

1. Introduction

Due to increased industrialization, the production of anthropogenic CO_2 is increasing[1] and the fate of this greenhouse gas has become a major concern.[2] On the other hand, about half of the primary carbon production is due to algal photosynthesis[3–5] and CO_2 sequestration by phytoplankton has thus a considerable impact on the climate.[6–14] Therefore, for realizing the impact of future environmental conditions, it is crucial to quantitatively understand the fixation of CO_2 into phytoplankton biomass. It has also been found that the chemical environment effects the biomass production and therefore the amount of fixed CO_2.[15–18] Hence, in order to quantify the transformation process, the surrounding chemical environment and its interaction with phytoplankton need to be investigated.

Marine microalgae's carbon sequestration occurs *via* two pathways:[11] (i) uptake of dissolved $CO_{2(aq)}$ and (ii) uptake of HCO_3^- which is produced *via* $CO_{2(g)} \rightarrow CO_{2(aq)} + H_2O \rightleftharpoons H_2CO_3 \rightleftharpoons HCO_3^- + H^+$. This study only focuses on (ii), *i.e.* on the sequestration of HCO_3^-. Experimental analyses of HCO_3^- concentrations remaining in an ecosystem would enable the quantitation of carbon sequestration. However, such measurements are challenging because in ecosystems often 10^5–10^7 cells per mL exist. These cells (typical size 5–20 μm[19]) only access HCO_3^- in their immediate, microscopic surroundings and thereby create a highly inhomogeneous concentration distribution. Computer models on the other hand can be tuned to relevant spatial resolutions and physiological parameters. In this study, the fixation of atmospheric CO_2 into algal biomass has been quantitatively modeled by linking all the interactions

University of Tennessee, Department of Chemistry, Knoxville, TN 37996, USA. E-mail: fvogt@utk.edu; Fax: +1 (865) 974-3465

†Electronic supplementary information (ESI) available. See DOI: 10.1039/c7an01054k

involved in the transformation process. From an analytical perspective, such an integrated approach can provide a novel framework to investigate this experimentally inaccessible environmental system.

A novel modeling methodology is presented that describes all chemical processes from dissolution of atmospheric CO_2, HCO_3^- formation and transport within an aqueous ecosystem, microalgae species-specific HCO_3^- uptake, nutrient competition among different species,[20,21] and HCO_3^- utilization for biomass production. The model has been developed to simulate the microscopic ecosystem with the aim of quantifying the algal biomass as a function of environmental conditions. Since the model links HCO_3^- concentrations with the produced biomass, this procedure also enables determining a HCO_3^- distribution, which itself is difficult to probe, *via* a property that can easily be measured. Therefore, model validation has been accomplished by comparing predicted cell concentrations with experimental flow cytometry measurements. The comparison against flow cytometry experiments then allows for an assessment of the model's performance and validity. Since the cells respond to their micro-environment as opposed to culture-average concentrations, the approach presented here gains a much more accurate assessment of the true conditions the cells experience. Therefore, quantitative statements derived by means of our modeling approach are more realistic and accurate. For experimental comparison, microalgae cultures of two species were grown under a series of different atmospheric CO_2 conditions.[22] As an additional aspect, these microalgae species were cultured individually as well as together which then enabled investigating competition impacts on the biomass production. Once validated, an application of such a model was presented to analyze the long term capacity of phytoplankton to transform atmospheric CO_2 into algal biomass.

2. Materials and methods

2.1. Theory

To link all the aforementioned steps leading from atmospheric CO_2 to microalgal biomass, the methodology 'concentration field' $c(\mathbf{x},t)$ has been introduced here. This concentration field is determined by four terms:

(i) A 'compound source' $S(\mathbf{x},t)$, *i.e.* the dissolution of atmospheric CO_2 into the aqueous phase and its subsequent reaction to HCO_3^- (also see the ESI†)

(ii) A 'transport term' $T(\mathbf{x},t)$ which comprises diffusion and advection of HCO_3^- within the aqueous phase

(iii) A 'compound drain' $D(\mathbf{x},t)$, *i.e.* microalgae's uptake of HCO_3^- out of the concentration field $c(\mathbf{x},t)$. $D(\mathbf{x},t)$ has to reflect that every microalgae species has specific compound uptake characteristics which may depend on $c(\mathbf{x},t)$ itself and potentially on the presence of competing species.

(iv) A 'utilization term' which describes how microalgae use this sequestered compound to produce new biomass. This was also anticipated to be species specific.

Terms (i) and (ii) describe the pathway by which HCO_3^- reaches the cells. Terms (iii) and (iv) model the actual chemical transformation from an inorganic compound into microalgal biomass. As $c(\mathbf{x},t)$ is space- and time-dependent, it is being expressed as a 3-dimensional partial differential equation (PDE) which must be numerically solved:

$$\frac{\partial c(\mathbf{x},t)}{\partial t} = S(\mathbf{x},t) + T(\mathbf{x},t) + D(\mathbf{x},t) \quad (1)$$

In order to keep modeling steps straightforward, algae cultures were considered to be stored in a box-shaped container rather than an odd-shaped Erlenmeyer flask.

2.1.1. The source term $S(\mathbf{x},t)$. All microalgae cultures were grown in open bottles protected by a cotton plug. Into these bottles' headspace, well-defined CO_2 concentrations had been provided[22] which then produced HCO_3^- in the aqueous phase (see the ESI†). Therefore, the source, $S(\mathbf{x},t)$, is spatially restricted to the interface between the atmosphere and the liquid culturing medium. Consequently, $S(\mathbf{x},t)$ has been expressed as a Dirichlet boundary condition $S(\mathbf{x}|_{\text{top surface}}, t) = f(pCO_2,\ldots) = c(\mathbf{x}|_{\text{top surface}}, t)$. For the container's remaining five walls, $S(\mathbf{x}|_{\text{walls except top}}, t) = 0$ and thus Neumann boundary conditions $\left.\frac{\partial c(\mathbf{x},t)}{\partial \mathbf{x}}\right|_{\text{walls except top}} = 0$ were implemented.

2.1.2. The transport term $T(\mathbf{x},t)$. Compound transport within an ecosystem is governed by diffusion and advection. The diffusion mechanism is defined by Fick's second law, *i.e.* $\left.\frac{\partial c(\mathbf{x},t)}{\partial t}\right|_{\text{diffusion}} = \kappa \cdot \nabla^2 c(\mathbf{x},t)$. The diffusion coefficient κ of HCO_3^- as determined in ref. 23 has been utilized in this study. In this modeling application, κ is assumed to be independent of temporal and spatial factors. Compound transport due to advection is described by $\left.\frac{\partial c(\mathbf{x},t)}{\partial t}\right|_{\text{advection}} = \nabla\cdot(\mathbf{v}(\mathbf{x},t)\cdot c(\mathbf{x},t))$ where $\mathbf{v}(\mathbf{x},t)$ is the velocity of the medium. The net compound transport is a combination of these two mechanisms *i.e.* $T(\mathbf{x},t) = \left.\frac{\partial c(\mathbf{x},t)}{\partial t}\right|_{\text{diffusion}} + \left.\frac{\partial c(\mathbf{x},t)}{\partial t}\right|_{\text{advection}}$. For this study, only diffusion has been considered though since the cell cultures were not mechanically moved and were at a homogeneous temperature. In conclusion:

$$T(\mathbf{x},t) = \left.\frac{\partial c(\mathbf{x},t)}{\partial t}\right|_{\text{diffusion}} = \kappa\cdot\nabla^2 c(\mathbf{x},t). \quad (2)$$

2.1.3. The drain term $D(\mathbf{x},t)$. In order to produce another microalgae cell, a cell located at $\mathbf{x}_0$ requires nutrients which it drains from the concentration field $c(\mathbf{x}_0,t)$ immediately surrounding it. Several quantitative models have been proposed for describing this phytoplankton based nutrient uptake for cell production.[24–33] For this modeling application, the classic Michaelis–Menten kinetics (MM)[27] has been chosen to characterize the nutrient uptake mechanism. MM describes a cell's nutrient uptake rate as $u_R = \frac{U_{max}\cdot c(\mathbf{x}_0,t)}{\alpha + c(\mathbf{x}_0,t)}$ with U_{max} denoting the maximum uptake rate and α representing the cell's nutri-

ent affinity (or 'half-saturation constant').[34] When, over time, the cells are being produced at x_0, a total of $N(x_0,t)$ cells results which deplete the concentration field according to $\frac{dc(x_0,t)}{dt} = -u_R \cdot N(x_0,t) = -\frac{U_{max} \cdot c(x_0,t)}{\alpha + c(x_0,t)} \cdot N(x_0,t) = D(x_0,t)$ and thereby establish the drain term for a single species culture which can be expanded to describe the drain performed by multiple species.

The relationship between nutrient concentration and its transformation into algal biomass was proposed by Monod.[28] In order to describe the cell production, *i.e.* $\frac{dN(x_0,t)}{dt}$, Monod introduced a 'nutrient efficiency' β as the number of cells produced per unit of the nutrient taken up. Thus, $N(x_0,t)$ cells consume the resource at the rate $u_R \cdot N(x_0,t)$ and therefore, the cell count increases by $\frac{dN(x_0,t)}{dt} = \beta \cdot u_R(t) \cdot N(x_0,t)$.

Expanding these two considerations to Q species located at x_0, all of which simultaneously drain $c(x_0,t)$, leads to a system of $Q+1$ ordinary differential equations (ODEs) (3):

$$\begin{aligned} D(x_0,t) &= \frac{dc(x_0,t)}{dt} = -\sum_{q=1}^{Q} \frac{U_{max_q} \cdot c(x_0,t)}{\alpha_q + c(x_0,t)} \cdot N_q(x_0,t) \\ \frac{dN_q(x_0,t)}{dt} &= \beta_q \cdot \frac{U_{max_q} \cdot c(x_0,t)}{\alpha_q + c(x_0,t)} \cdot N_q(x_0,t) \end{aligned} \quad (3)$$

Fusing the top eqn (3) and (2) into (1) together with the source term $S(x,t)$ (section 2.1.1) describes how the concentration field at x_0 changes over time. Since the considerations leading to (3) are valid for any x_0, they are valid at all x. Thus, (4 top) describes how atmospheric CO_2 is sunk into an ecosystem. The equation (4 bottom) explains for all locations x the utilization of this nutrient to produce, over time, $N_{q=1,\ldots Q}$ cells of Q microalgae species. Integration of the concentration field and biomass produced after nutrient utilization together into (4) allows the quantitative analysis of the sequestration process. In conclusion, solving the system of $Q+1$ partial differential eqn (4) models the transformation of atmospheric CO_2 into microalgal biomass.

$$\begin{aligned} \frac{\partial c(x,t)}{\partial t} &= S(x,t) + \kappa \cdot \nabla^2 c(x,t) - \sum_{q=1}^{Q} \frac{U_{max_q} \cdot c(x,t)}{\alpha_q + c(x,t)} \cdot N_q(x,t) \\ \frac{\partial N_q(x,t)}{\partial t} &= \beta_q \cdot \frac{U_{max_q} \cdot c(x,t)}{\alpha_q + c(x,t)} \cdot N_q(x,t) \quad \text{with } q = 1,\ldots,Q \end{aligned} \quad (4)$$

2.2. Software tools and computations

The modeling was carried out on a computer operating under CentOS 7 that featured two Intel Xeon processors E5-2650 v3 (2 × 10 cores) and 128 GB RAM. The system of PDEs (4) has been solved on a grid of size $x \times y \times z = 1024 \times 1024 \times 32$ which, in conjunction with the experimentally realized culture volume of 100 mL, translated into the model's spatial resolution of 100 μm in either direction. Solutions of (4) have been computed by means of the 'Portable, Extensible Toolkit for Scientific Computation' (PETSc)[35] software package which was augmented by the SUNDIALS library.[36] PETSc handles large scale linear and nonlinear problems through the 'Krylov Space method' (KSP; used here for initializing $c(x,t=0)$; see next paragraph) and the 'simplified nonlinear equation solver' (SNES; used to solve (4) in time steps), respectively. For core-to-core and/or processor-to-processor communication, PETSc relies on the Message Passing Interface (MPI).[37] For this study the openMPI implementation version 1.10.0[38] has been utilized in conjunction with the g++ compiler version 5.2.0.[39]

Prior to solving the PDE system (4), $c(x,t)$ needed to be initialized which has been done *via* the following procedure: first, the concentration field is assumed to be void of HCO_3^-; however, a user-selected CO_2-concentration is present in the 'atmosphere' on top of the 'liquid culturing medium'. Through the gas–liquid interface, atmospheric CO_2 partitions into the liquid phase and creates a $[HCO_3^-] = c(x|_{top\ surface}, t) = f(pCO_2,\ldots)$ (see the ESI†). This top layer of HCO_3^- acts as the HCO_3^--source $S(x,t)$ for the entire concentration field. The aforementioned KSP solver is then applied to determine a steady-state solution of the diffusion equation $\frac{\partial c(x,t)}{\partial t} = \kappa \cdot \nabla^2 c(x,t)$. This steady-state solution serves as initialization of the concentration field, *i.e.* $c(x,t=0)$. Then, at $t=0$, the nutrient uptake of the microalgae cells, *i.e.* $D(x,t)$, is 'turned on' and the PETSc's time stepper (TS) library advances the concentration field stepwise in time as microalgae consume HCO_3^-. At each time point, SNES is employed for solving (4). This HCO_3^--sequestration creates localized and microscopic concentration depressions which are replenished by the transport term $T(x,t)$.

For a reliable comparison of predicted and experimentally determined cell numbers, both need to be initialized with the same $N_{q=1,\ldots,Q}(x,t=0)$ distributed in the same way across the culture volume or any difference would amplify over time. Thus, the first experimental cell count is chosen as an 'inoculation cell number' for the modeling. In simulations, this cell number is homogeneously distributed among all grid points. However, compared to an 'inner' grid point, grid points on a container wall only got half that number assigned, grid points on a container edge a quarter, and corner grid points one eighth. Experimentally, a homogeneous distribution of $N_{q=1,\ldots,Q}(x,t=0)$ has been ensured by swirling the Erlenmeyer flask right after inoculation. Once the boundary conditions are implemented and model parameters are initialized, solutions of PDE system (4) are calculated at different atmospheric CO_2 levels for experimental model validation.

2.3. Experiments for model validation

Model validation has been based on comparing experimentally generated, species-specific quantities of microalgal biomasses $N_{q=1,\ldots,Q}$ to those predicted by eqn (4). For this study, two marine microalgae species were selected, *i.e. Dunaliella salina* and *Nannochloropsis oculata* (supplier: http://www.utex.org). *D. salina* is a well-characterized species[40] and *N. oculata* is

known for its considerable chemical response to changing the HCO_3^- levels.[41] These two different microalgae species have been included in this study to demonstrate the model's general validity and to investigate competition impacts on the biomass production.

Microalgae cultures were provided with different levels of HCO_3^- either by dissolving $NaHCO_3$ into the culturing medium (section 2.3.1) or by flushing a certain CO_2 concentration into a culture's headspace (section 2.3.2), respectively. All other nutrients were supplied *via* the culturing medium ('Enriched Seawater, Artificial Water', ESAW) at concentrations in accordance with the standard protocol.[42,43] Microalgae concentrations in the resulting cultures were measured by means of flow cytometry (Guava easyCyte equipped with 488 nm laser). Both microalgae species show a unique red fluorescence which facilitated an accurate cell count. The clearly different sizes of *D. salina* and *N. oculata* ensured a reliable quantitation for both species even in mixtures. Furthermore, six replicate flow cytometry data were extracted from the same culture and analyzed in order to assess the reproducibility of these cell counts. From these replicated analyses, the error bars shown in subsequent graphs comparing measured *versus* predicted cell counts were derived.

2.3.1. Culture preparation for determining nutrient uptake characteristics. Prior to modeling (4), values for the species-dependent nutrient uptake characteristics α, β, and U_{max} need to be determined experimentally. It has been hypothesized that these parameters depend on the species, on the HCO_3^- concentration, and on the presence of nutrient competitors. For each species in individual and mixed cultures, these parameters' values have been determined for a series of fixed initial HCO_3^- concentrations (0.518 mM, 1.035 mM, 1.553 mM, 2.071 mM, 2.919 mM, 3.443 mM) by means of growth curves (Fig. 1 in ref. 44).‡ For extracting α, β, and U_{max} from growth curves, a method[44] has been employed which combines solving the ODE system (MM,[27] Monod[28])

$$\frac{dc(t)}{dt} = -\frac{U_{max}\cdot c(t)}{\alpha + c(t)}\cdot N(t)$$

$$\frac{dN(t)}{dt} = \beta\cdot\frac{U_{max}\cdot c(t)}{\alpha + c(t)}\cdot N(t)$$

with a nonlinear least-squares regression step that estimates values for α, β, and U_{max} such that the numerical solution of the ODE system is optimum in a least-squares sense. Once α, β, and U_{max} had been determined for all HCO_3^- concentrations and for all three culture types (*D. salina*, *N. oculata*, and *D. salina* + *N. oculata*), first and second order polynomials in $[HCO_3^-]$ were fitted to these data points (Fig. 1). The resulting polynomials such as $\alpha([HCO_3^-]) = \theta_0 + \theta_1\cdot[HCO_3^-] + \theta_2\cdot[HCO_3^-]^2$ were then incorporated into the modeling software evaluating (4) to describe nutrient uptake characteristics as a continuous function of $[HCO_3^-] = c(x,t)$. Whether or not a zeroth, first, or second order polynomial is the best has been tested by means of an Analysis of Variance (ANOVA, confidence level 95%[45]). First, Fig. 1 reveals that for all three culture types, all three parameters exhibit a strong dependency on the HCO_3^--concentration which clearly justifies incorporating $\alpha([HCO_3^-])$, $\beta([HCO_3^-])$, and $U_{max}([HCO_3^-])$ into (4) as HCO_3^--dependent functions rather than constants.

The impact of nutrient competition on the growth parameters α, β, and U_{max} can be deduced by comparing the following panels in Fig. 1: A–C (*D. salina* individual) to D–F (*D. salina* in mixtures) as well as G–I (*N. oculata* individual) to J–L (*N. oculata* in mixtures). Values for the half saturation constant, α, for both species individually and in mixtures were in the same order of magnitude and with the exception of pure *D. salina* at high concentration, α-values were found to be increasing with the HCO_3^--concentration. ANOVA implied a linear relationship for *D. salina* in mixed culture, while nonlinearity was significant for the other three situations. The nutrient efficiency, β, for *D. salina* was one order of magnitude lower than that for *N. oculata* in individual cultures. This is assumed to be the reason why a higher cell concentration of *N. oculata* has been observed compared to *D. salina* (*cf.* section 3). Moreover, competition for nutrients influenced both the shape and the magnitude of concentration dependent β-values for *D. salina*. On the other hand, *N. oculata* exhibited a similar trend in β-values with a slight increase in magnitude. Concentration dependency of the maximum uptake rate, U_{max}, for both single-species cultures was in comparable order of magnitude. For both species in mixed cultures, there was a significant decrease in the U_{max} values compared to the corresponding single-species cultures. Moreover, the functional relation between U_{max} and $[HCO_3^-]$ was found to be very similar between both single-species cultures as well as for both species in mixtures but very different for single- and mixed-species cultures.

2.3.2. Culture preparation for model validation. For a model validation purpose, experimental data were required which have been acquired from microalgae that were exposed to a known chemical steady-state environment. In particular the concentration of atmospheric CO_2 in the cultures' headspace needed to be well-defined and stable over the course of several days because only then the atmospheric conditions can be related to the microalgal biomass produced. By means of two mass flow controllers (Sierra Instruments), CO_2 had been mixed with synthetic air resulting in gas mixtures containing 300 ppm, 350 ppm, 400 ppm, 450 ppm, and 500 ppm CO_2, respectively, which were then continuously flushed through five different cultures' headspaces. These concentrations were chosen to simulate pre-industrial, current, and potential future atmospheric conditions. All other nutrients the cells require were provided *via* the culturing medium (ESAW). In order to replenish consumed, aqueous phase nutrients, fresh ESAW was slowly but continuously dripped into the Erlenmeyer flasks which were equipped with an over-

‡Growth curves describe cell counts or cell concentrations over time and are usually of sigmoidal shape.

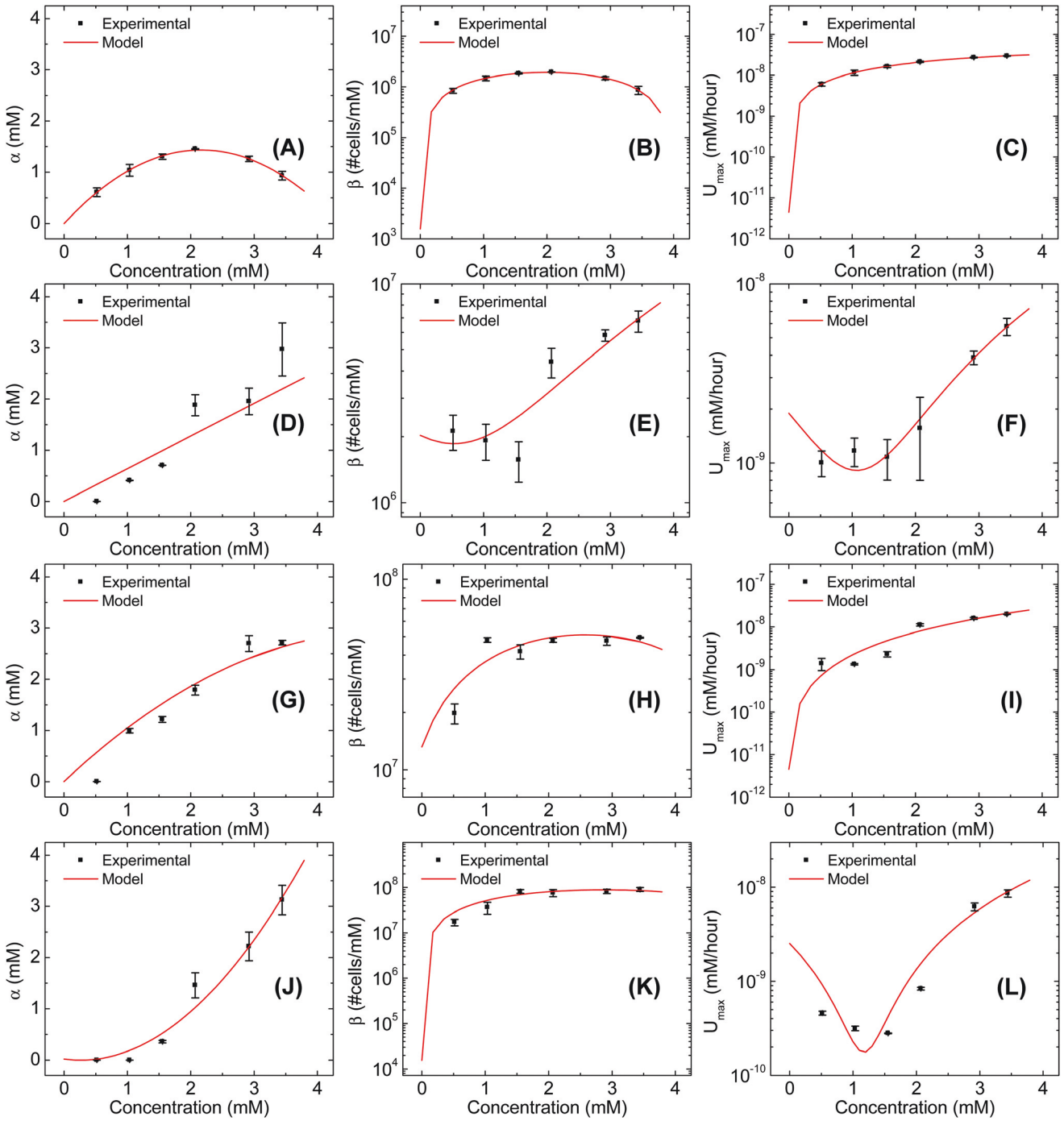

Fig. 1 Concentration dependency of the parameters α, β, and U_{max}, which describe the cells' nutrient uptake, for individual *D. salina* (A–C) and individual *N. oculata* (G–I) cultures as well as their counterparts determined in binary mixtures of *D. salina* (D–F) plus *N. oculata* (J–L). Since nonlinear regression cannot determine unique solutions,[46] nonlinear regression calculations have been repeated five times leading to the error bars.

flow through which consumed medium was released. Over the course of several days, small aliquots of these cultures were extracted for the determination of a culture's current cell concentrations by means of flow cytometry. These experimental data were then compared to cell concentrations predicted by means of (4).

3. Results and discussion – model validation

The concentration field $c(\mathbf{x},t)$ and species-specific cell counts $N_{q=1,\ldots,Q}(\mathbf{x},t)$ have been computed from (4) for the same

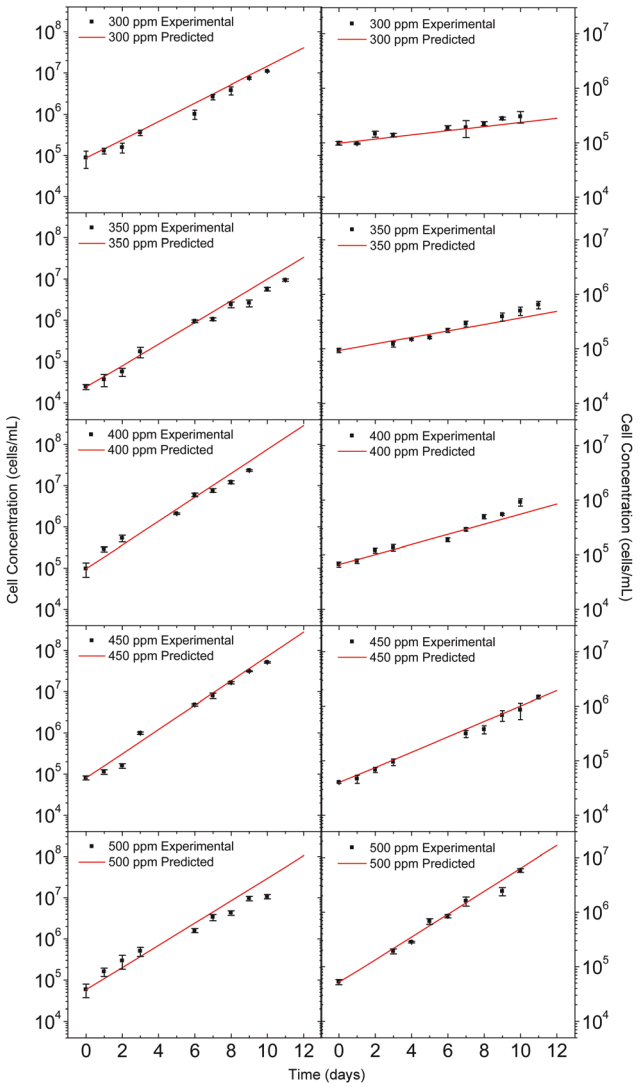

Fig. 2 Model validation with experimental data for *D. salina* in individual species cultures (left column) and binary species mixtures (right column) at different atmospheric CO_2-concentrations (300–500 ppm).

environmental conditions under which the real-world microalgae were grown (see section 2.3.2). PETSc's time-stepper (section 2.2) advanced $c(\mathbf{x},t)$ to the same points of time at which the cultures were subjected to flow cytometry experiments.§ The model predicted absolute cell numbers which were converted into cell concentration utilizing the known culture volume. This procedure enabled a direct comparison between predicted and experimentally obtained cell concentrations.

§ Note that it is important to utilize the single-species version of the species-specific nutrient uptake characteristics a_q, β_q, and U_{max_q} (section 2.3.1) for single species cultures and their multi-species counterparts for species mixtures (see Fig. 1).

3.1. Modeling of *Dunaliella salina* production

The left column of Fig. 2 compares experimental and predicted cell concentrations obtained for single-species cultures grown at different atmospheric CO_2 concentrations. For all CO_2 situations a convincing agreement has been found which indicates that the PDE (4) is a good description of the transformation of atmospheric CO_2 into *D. salina* biomass. This agreement between theory and experiment stretches over the course of ten days which demonstrated that (4) not only properly describes quantities but also explains the dynamics of *D. salina* production. The right column depicts equivalent information but in these cultures, *D. salina* was competing with *N. oculata*. Again the predictions are capable of explaining the experimental data well. For all investigated atmospheric CO_2 concentrations, the cell concentration is approximately one order of magnitude lower in the binary species cultures

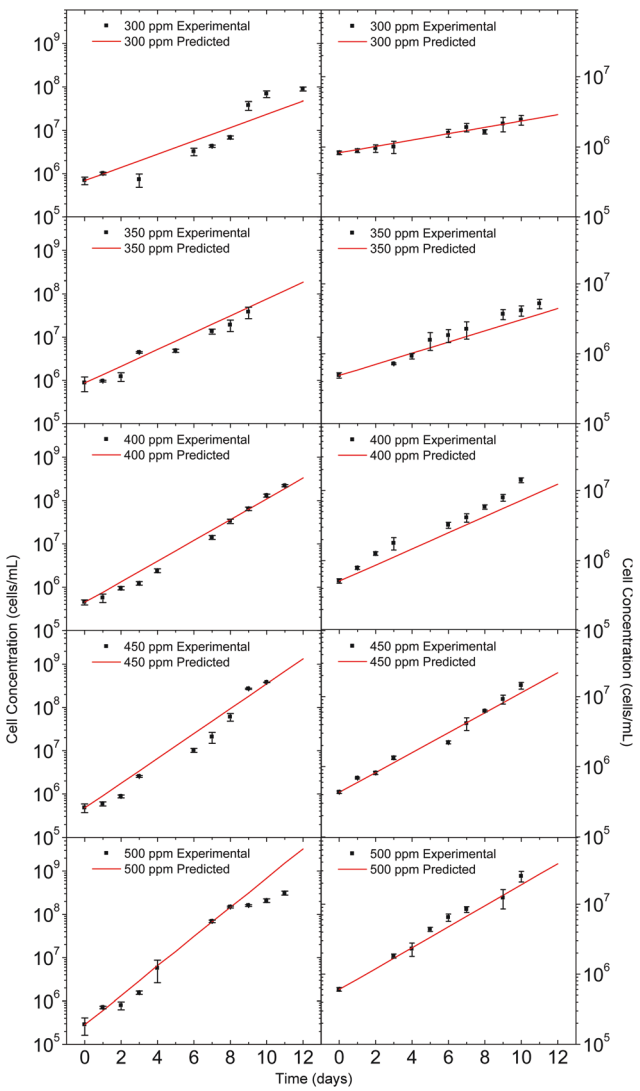

Fig. 3 Model validation with experimental data for *N. oculata* in individual species cultures (left column) and binary species mixtures (right column) at different atmospheric CO_2-concentrations (300–500 ppm).

compared to sole *D. salina* cultures. The decrease in the maximum uptake rate values (U_{max}) in mixed cultures (Fig. 1C *vs.* F) is possibly responsible for these reduced cell concentrations. It is also noticeable that compared to pure *D. salina* cultures, in such competition situations, the CO_2 concentration does have a pronounced impact on the resulting cell concentration which increases with [CO_2].

3.2. Modeling of *Nannochloropsis oculata* production

Fig. 3 depicts information equivalent to Fig. 2 but for *N. oculata*. First, it is notable that the model (4) describes the production of *N. oculata* cells well, too, and that the dynamics of cell production is again in good agreement with the experiment. This was found for single-species *N. oculata* cultures (Fig. 3 left column) as well as for *N. oculata* in mixtures with *D. salina* (Fig. 3 right column). For all investigated atmospheric CO_2 concentrations, the quantity of *N. oculata* biomass is considerably higher than that for *D. salina* (*cf.* left columns of Fig. 3 and 2). This can be explained by *N. oculata*'s higher nutrient efficiency value, β, compared to *D. salina*'s (Fig. 1H *vs.* B) which implies that *N. oculata* produces more cells per nutrient unit. The cell concentration of *N. oculata* in binary mixtures (Fig. 3 right column) is approximately one order of magnitude lower compared to single-species culture. This can be explained by the reduced values of the maximum uptake rate, U_{max}, for *N. oculata* in binary mixtures with *D. salina* compared to cultures containing exclusively *N. oculata* cells (compare Fig. 1L *vs.* I). It is also evident that, in contrast to single *D. salina* cultures, the atmospheric CO_2 concentration has a considerable impact on the *N. oculata* biomass production in both single-species and binary mixed cultures.

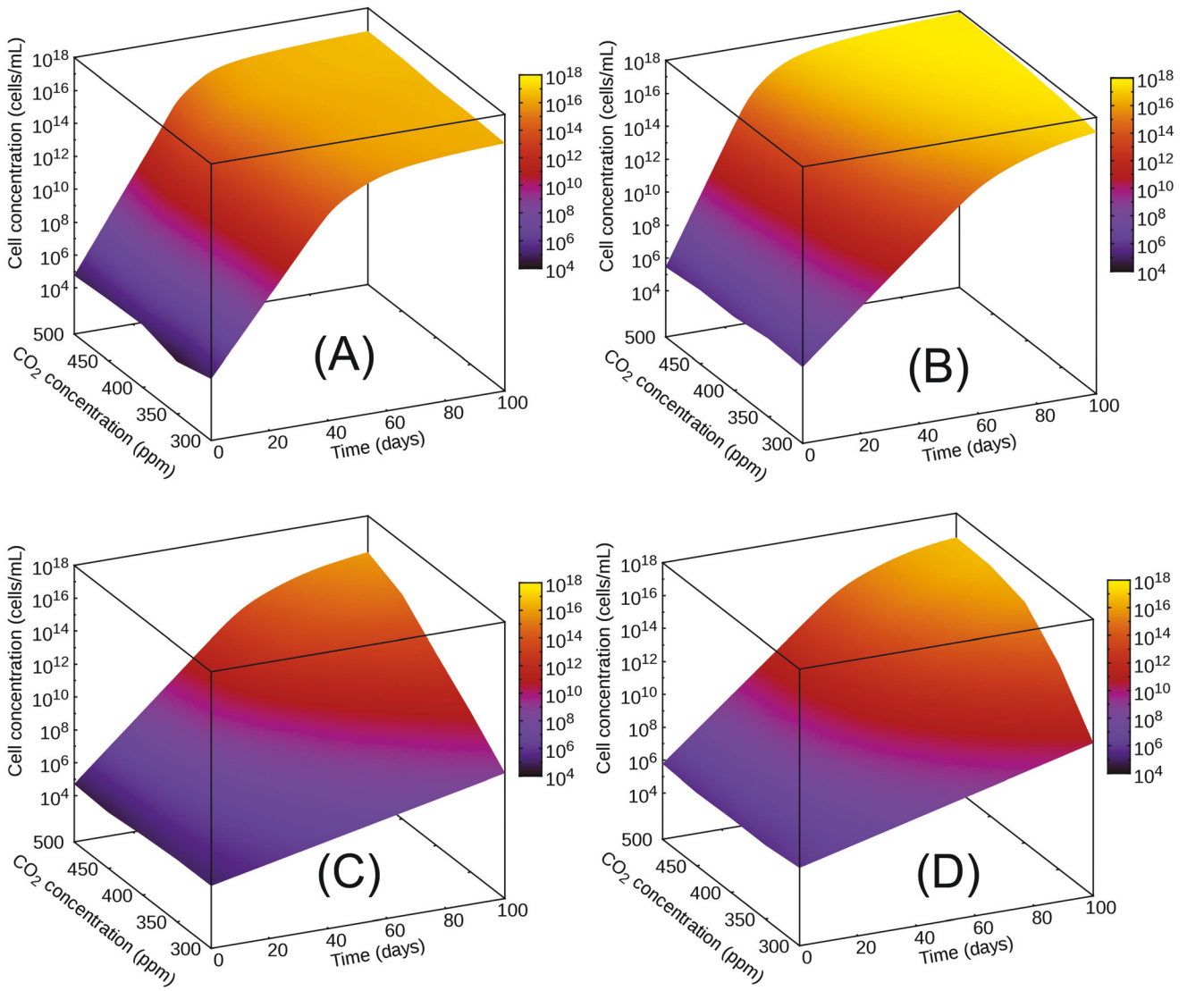

Fig. 4 Predicted cell concentrations increasing over time produced by different levels of atmospheric CO_2 – (A) *D. salina* grown individually; (B) *N. oculata* grown individually; (C) *D. salina* in competition with *N. oculata*; (D) *N. oculata* in competition with *D. salina*; note the $\log_{10}$-scale on the *z*-axis.

Hence, it can be concluded that for the chosen species the concentration field method properly describes the main driving forces behind the transformation of atmospheric CO_2 into microalgal biomass. This assessment holds for individually cultured as well as for competing species.

3.3. Assessing a culture's long-term capability for CO_2 sequestration

For assessing phytoplankton's CO_2 sinking capacities, it has been investigated whether a microalgae culture reaches an upper limit in cell numbers or whether it continues growing unrestrictedly. If, over time, the cell production slows down, so does the increase of sequestered CO_2. If a culture's growth is unrestricted, its CO_2 sinking capacity increases unimpededly. Model (4) has been employed for long-term predictions of produced cell numbers. These simulations have been performed for a period of 100 days under different atmospheric CO_2 concentrations ranging from 300–500 ppm.

Fig. 4 displays predicted cell concentrations over time as a function of atmospheric CO_2 concentration. Four scenarios were considered, *i.e. D. salina* and *N. oculata* growing individually as well as both species competing with each other. From Fig. 4(A and B), it can be concluded that both species in individual cultures exhibit a qualitatively similar behavior with *N. oculata* having a faster growth and a stronger dependency on the CO_2 concentration. Most importantly though, it is noticeable that both species' growth slows down as indicated by the surfaces becoming much flatter at later times. Based on the flatness of these plateaus, it can be concluded that *D. salina* slows down more than *N. oculata*. Moreover, *N. oculata* cultured at high CO_2 concentrations seems to slow down more and faster compared to low CO_2 concentrations. *D. salina*'s slowdown on the other hand features a much lower dependency on the CO_2 concentration. In conclusion, the main findings of this analysis are that overall the production of new cells slows down with time. This fact means that the CO_2 sequestration at later points of time does not increase as much as at earlier times. In other words, an increase in anthropogenic CO_2 release may outweigh an increase in phytoplankton production.

In a competition situation (Fig. 4C and D),¶ the cell production by both species generally shows a much stronger dependency on the CO_2 concentration. It also is considerably lower than in the corresponding single-species cultures (Fig. 4A and B). Apparently, competition suppresses cell growth with *D. salina* being the more impacted species. Moreover, the growth rates are lower in a competition scenario as indicated by the shallower slopes of the surfaces in time-direction. It is also obvious, that over time cell production tends to slow down but much less than in the single species cases. Nonetheless, it is reasonable to assume that these surfaces reach a plateau at times >100 days. From these findings, it may be concluded that mixed species cultures sequester less CO_2 than a single-species culture. This is another aspect to consider when assessing phytoplankton's CO_2 sequestration capacity.

4. Conclusions

A modeling method has been developed to describe phytoplankton based CO_2 sequestration and thus the transformation of this greenhouse gas into algal biomass. Modeling comprises of several steps, *i.e.* CO_2 partitioning from the atmosphere into bodies of water, its conversion into HCO_3^-, bicarbonate's transport from source to consumers, and species-specific compound uptake for biomass production. All but the last step have been described by chemical kinetics and mass transport. The nutrient (HCO_3^-) uptake mechanism by microalgae cells has been realized through Michaelis–Menten kinetics. Subsequent nutrient utilization has been described by the Monod model which quantitatively relates the sequestration of nutrients to biomass production. Furthermore, the model was designed to incorporate multiple microalgae species in order to describe real-world ecosystems where several species compete for a common nutrient source. Through this novel modeling methodology, transformation of an inorganic compound into algal biomass can be assessed quantitatively.

For modeling purposes, three parameters that describe the cells' nutrient uptake characteristics had to be determined experimentally. It was found that these parameters depend on the species, the nutrient availability, and the presence of nutrient competitors. With these concentration dependent parameters describing the situation specific dynamics of nutrient uptake, species-specific biomass production could be expressed as a system of partial differential equations (PDEs). Numerically solving this PDE system then predicted the quantities of produced microalgae cells over time.

For experimental validation, two microalgae species (*Dunaliella salina* and *Nannochloropsis oculata*) had been chosen and were cultured individually and in a competition situation. Flow cytometry was used to measure experimental cell concentration over the course of ten days for both single-species and binary species cultures. For all three culture types (single *D. salina*, single *N. oculata*, and *D. salina* + *N. oculata*) and for all analyzed atmospheric CO_2-concentrations (300 ppm–500 ppm) a very good agreement between experiment and model has been found.

After confirming that the novel modeling approach can with high accuracy predict the species-dependent production of microalgae cells, this model has been applied to study long-term trends in cell production. Motivation for this is to determine whether the cell production continues unimpededly or

¶ For an assessment of competition impacts, *e.g. D. salina* in single-species cultures *versus D. salina* in mixtures, experimental data cannot be used as inoculating two separate cultures with the same number of cells $\left(N_q^{\text{single}} = N_q^{\text{mixture}} \text{ at } t = 0\right)$ is essentially impossible. Yet, both cultures need to be started with an identical number of cells as even small differences in cell concentration at $t = 0$ would amplify over time and thereby prohibit a realistic assessment of competition impacts. Nutrient competition can be studied *in silico* (4) though as an identical number of inoculated cells in two cultures can be simulated.

slows down as the culture grows. If the cell production is not slowed down over time, neither is the phytoplankton-based CO_2 sequestration. If biomass generation does slow down, the CO_2-storage capacity of microalgae diminishes. Simulations determined that the latter is the case for all considered atmospheric CO_2 concentrations and all three culture types. One potential consequence of this fact is that future increases of anthropogenic CO_2 releases may not be counterbalanced by growing phytoplankton cultures.

Moreover, it was found that nutrient competition among different species considerably reduces the number of cells produced. This means that a real-world, mixed species culture has a lower CO_2-sinking capability than the individual species. There are indications that the cell production in mixed-species cultures also slows down over time but that this slowdown is delayed. Again, a potential consequence is that mixed species cultures need to be considered when assessing phytoplankton's CO_2 sequestration capacity.

Ongoing research is expanding the aforementioned modeling software describing the biomass production to actually determining quantities of sequestered CO_2 and other inorganic compounds. For model and software validation, experimental setups need to be developed for online measuring the average concentrations of the said inorganics in the aqueous phase and the headspace of a culture. This has to be performed for multiple concentrations per compound.

Ultimately, the experimental investigations of dynamic adaptation of phytoplankton to a chemically changing environment and the modeling software determining the quantities of sequestered inorganic compounds need to be fused together. This will then result in a comprehensive, quantitative description and prediction of future responses of marine environments to anthropogenic pollution.

Conflicts of interest

There are no conflicts to declare.

Acknowledgements

This work was partially supported by the National Science Foundation under CHE-1710175. The authors are grateful to Erik Zinser and Benjamin Calfee, Department of Microbiology at the University of Tennessee, for their guidance in performing flow cytometry experiments and for granting us access to their instrument.

References

1 G. P. Peters, G. Marland, C. Le Quere, T. Boden, J. G. Canadell and M. R. Raupach, *Nat. Clim. Change*, 2012, **2**, 2–4.
2 M. Eby, K. Zickfeld, A. Montenegro, D. Archer, K. J. Meissner and A. J. Weaver, *J. Clim.*, 2009, **22**, 2501–2511.
3 J. Raven, M. Giordano, J. Beardall and S. Maberly, *Photosynth. Res.*, 2011, 281–296.
4 M. Behrenfeld, R. O'Malley, D. Siegel, C. McClain, J. Sarmiento, G. Feldman, A. Milligan, P. Falkowski, R. Letelier and E. Boss, *Nature*, 2006, **444**, 752–755.
5 C. B. Field, M. J. Behrenfeld, J. T. Randerson and P. Falkowski, *Science*, 1998, **281**, 237–240.
6 G. C. Hays, A. J. Richardson and C. Robinson, *Trends Ecol. Evol.*, 2005, **20**, 337–344.
7 R. Bardgett, C. Freeman and N. Ostle, *ISME J.*, 2008, **2**, 805–814.
8 J. Berges and P. Falkowski, *Limnol. Oceanogr.*, 1998, **43**, 129–135.
9 S. Sanudo-Wilhelmy, A. Kustka, C. Gobler, D. Hutchins, M. Yang, K. Lwiza and J. Burns, *Nature*, 2001, 66–69.
10 S. Burkhardt, I. Zondervan and U. Riebesell, *Limnol. Oceanogr.*, 1999, **43**, 129–135.
11 M. Giordano, J. Beardall and J. A. Raven, *Annu. Rev. Plant Biol.*, 2005, **56**, 99–131.
12 E. Huertas, G. Navarro, S. Rodriguez-Galvez and L. Prieto, *Can. J. Bot.*, 2005, **83**, 929–940.
13 D. Bilanovic, A. Andargatchew, T. Kroeger and G. Shelef, *Energy Convers. Manage.*, 2009, **50**, 262–267.
14 J. Beardall, S. Stojkovic and S. Larsen, *Plant Ecol. Divers.*, 2009, **2**, 191–205.
15 G. Amoroso, D. Sültemeyer, C. Thyssen and H. P. Fock, *Plant Physiol.*, 1998, **116**, 193–201.
16 M. B. McConico and F. Vogt, *J. Chemom.*, 2013, **27**, 217–219.
17 U. Riebesell, *J. Oceanogr.*, 2004, **60**, 719–729.
18 F. Vogt and L. White, *Anal. Chim. Acta*, 2015, **867**, 18–28.
19 A. G. Dickson, C. L. Sabine and J. R. Christian, *Guide to Best Practices for Ocean CO_2 Measurements*, North Pacific Marine Science Organization, Sidney, British Columbia, 2007.
20 M. McConico and F. Vogt, *Anal. Lett.*, 2013, **46**, 2752–2766.
21 L. White, D. Martin, K. Witt and F. Vogt, *J. Chemom.*, 2014, **28**, 448–461.
22 Z. L. Ogburn and F. Vogt, *Anal. Chim. Acta*, 2017, **954**, 1–13.
23 R. E. Zeebe, *Geochim. Cosmochim. Acta*, 2011, **75**, 2483–2498.
24 J. A. Bonachela, M. Raghib and S. A. Levin, *Proc. Natl. Acad. Sci. U. S. A.*, 2011, **108**, 20633–20638.
25 C. A. Klausmeier, E. Litchman and S. A. Levin, *Limnol. Oceanogr.*, 2004, **49**, 1463–1470.
26 D. L. Aksnes and J. K. Egge, *Mar. Ecol.: Prog. Ser.*, 1991, **70**, 65–72.
27 U. Deichmann, S. Schuster, J. P. Mazat and A. Cornish-Bowden, *FEBS J.*, 2014, **281**, 435–463.
28 J. Monod, *Annu. Rev. Microbiol.*, 1949, **3**, 371–394.
29 R. C. Dugdale and J. J. Goering, *Limnol. Oceanogr.*, 1967, **12**, 196–206.
30 M. R. Droop, *J. Phycol.*, 1973, **9**, 264–272.
31 D. E. Burmaster, *Am. Nat.*, 1979, **113**, 123–134.

32 M. J. R. Fasham, H. W. Ducklow and S. M. Mckelvie, *J. Mar. Res.*, 1990, **48**, 591–639.
33 J. D. Haney and G. A. Jackson, *J. Plankton Res.*, 1996, **18**, 63–85.
34 R. W. Eppley, J. N. Rogers and J. J. McCarthy, *Limnol. Oceanogr.*, 1969, **14**, 912–920.
35 S. Balay, S. Abhyankar, M. F. Adams, J. Brown, P. Brune, K. Buschelman, L. Dalcin, V. Eijkhout, W. D. Gropp, D. Kaushik, M. Knepley, L. C. McInnes, K. Rupp, B. Smith, S. Zampini and H. Zhang, PETSc Web page, http://www.mcs.anl.gov/petsc, (accessed 6/23/2017).
36 A. Hindmarsh, P. Brown, K. Grant, S. Lee, R. Serban, D. Shumaker and C. Woodward, *ACM Trans. Math. Softw.*, 2005, **31**, 363–396.
37 P. S. Pacheco, *Parallel Programming with MPI*, Morgan Kaufmann Publishers Inc., 1996.
38 Open MPI Webpage, http://www.open-mpi.org/software/ompi/v1.10/, (accessed 10/4/2017).
39 GCC, the GNU Compiler Collection Webpage, https://www.gnu.org/software/gcc/, (accessed 6/23/2017).
40 A. Oren, *Saline Syst.*, 2005, **1**, 2.
41 S. Y. Chiu, C. Y. Kao, M. T. Tsai, S. C. Ong, C. H. Chen and C. S. Lin, *Bioresour. Technol.*, 2009, **100**, 833–838.
42 R. Anderson, *Algal Culturing Techniques*, Elsevier Academic Press, Burlington, MA, 2005.
43 J. A. Berges, D. J. Franklin and P. J. Harrison, *J. Phycol.*, 2001, **37**, 8.
44 F. Vogt and S. D. Fleming, *Anal. Lett.*, 2016, **49**, 2043–2051.
45 N. Draper and H. Smith, *Applies Regression Analysis*, J. Wiley, New York, 3rd edn, 1998.
46 F. Vogt, *J. Chemom.*, 2015, **29**, 71–79.